JOURNAL OF Materials CHEMISTRY

Electrochemical and multinuclear solid-state NMR studies of tin composite oxide glasses as anodes for Li ion batteries

Gillian R. Goward, Linda F. Nazar* and William P. Power*

Department of Chemistry, University of Waterloo, Waterloo, ON, Canada N2L 3G1

Received 17th February 2000, Accepted 2nd March 2000
Published on the Web 4th April 2000

Electrochemical and multi-nuclear solid-state NMR studies of various tin oxide and two tin composite oxide (TCO $Sn_{1.0}Al_{0.42}B_{0.56}P_{0.40}O_{3.6}$ and Sn-rich TCO $Sn_{1.5}Al_{0.42}B_{0.56}P_{0.40}O_{4.2}$) samples are described, which give a coherent picture of the different processes occurring within these systems. ^{6,7}Li NMR results demonstrate that the agglomeration of Li–Sn domains is inhibited in TCO; in contrast, in SnO, the aggregation of particles is observed. This difference results in part from the facile back-reaction between Sn and O. The interfacial energy of the most highly divided particles (TCO) allows the "back-reaction" of lithium with oxygen to be reversible at a lower potential than predicted from simple thermodynamic considerations that exclude surface energy contributions. Thus, the proximity and availability of oxygen in the host matrix may indirectly enhance the reversibility and cyclability of the cell in these materials, by "trapping the Sn particles". Aggregation may also be limited in TCO owing to the participation of the matrix observed by ^{27}Al, ^{31}P, and ^{11}B NMR, where reversible changes in the coordination environment are observed during lithium uptake and removal. The size-limiting role of the matrix ions is key to the enhanced electrochemical properties of the TCO glass. The initial rearrangement of the glass network is kinetically limited, as demonstrated by galvanostatic intermittent titration technique (GITT) experiments. The combined results of this study demonstrate the unique nature of the reaction between lithium and TCO.

Introduction

The lithium ion rechargeable battery relies on the simultaneous insertion/deinsertion of lithium ions and electrons into positive and negative electrode materials. The positive electrode (cathode) must insert Li at a relatively high potential *vs.* Li/Li^+; conversely the negative electrode (anode) must have a low binding energy for Li. Graphitic carbon was the first material used as the anode in Li ion batteries in 1992, and is still the material of choice today. Its inherent limitations, however, in both its gravimetric and volumetric capacity have resulted in a search for new materials that could supplant it in the next generation of devices. This search has been accelerated, in part, by the exciting reports of Li ion uptake by amorphous tin oxide glasses at low potential. A series of patents announced by Fuji[1] were followed by a report in *Science* in 1997, highlighting the electrochemical performance of an amorphous tin composite oxide (TCO) glass, $Sn_{1.0}B_{0.56}P_{0.4}Al_{0.42}O_{3.6}$.[2] Few details were provided at the time to explain the enhanced behaviour over that of SnO itself, however, although the role of tin as an "active centre" was implicated. Along with this, there has been renewed interest in multiphase Sb/Si/Sn materials,[3] new nanocomposite inactive/active materials which address the possibility of electrochemical lithium insertion into an active metal center which is embedded in a composite matrix other than an oxide,[4] and more recently, insertion into main group/transition metal intermetallics.[5]

The major difference between these types of material and the traditional graphitic carbon anode may relate to the mechanism of Li insertion. Lithium inserts topotactically between the graphitic carbon layers, up to a maximum capacity of C_6Li. This represents an intercalation process in which the only structural change is the reversible expansion of the interlayer spacing. The mechanism in the TCO glass is less clear. Since the original report by Fuji, several diffraction studies of the parent SnO_2 and SnO have been reported, outlining the possible reactions within the anode. The first step in Li uptake is unequivocally the formation of elemental Sn *via* reduction of the Sn(II) or Sn(IV) centers, *i.e.* $SnO_2+4Li^++4e^-\rightarrow Sn+2Li_2O$. Both elemental Sn (diffraction,[6] Raman,[7] and TEM/EDX)[8] and the formation of the Li_2O matrix (NMR)[9] have been directly detected.

As for the subsequent steps, it is known that lithium chemically reacts with tin at high temperature to form a series of stoichiometric compounds (line phases), which differ structurally from one another, and from tin metal.[10] In this reaction, which also occurs electrochemically,[11] and is enhanced at elevated temperatures, lithium insertion is accompanied by a volume increase of 676%.[12] Although theoretically reversible, this is not a topotactic reaction; there is also a substantial kinetic inhibition to Li incorporation. Tin metal itself is not a viable anode for this reason, as the volume changes are presumed to cause structural fracturing, particle breakdown and ultimately loss of contact with the current collector. In the case of the Fuji tin composite oxide, the promising electrochemical performance is considered to result from the presence of the inert oxide matrix which acts to prevent aggregation of the tin particles.[4]

The mechanism responsible for the large reversible capacity is proposed to be based on formation of these line phases ("alloys"), namely: $xLi^++Sn+xe^-\rightarrow Li_xSn$. Using *in-situ* X-ray diffraction, Courtney and Dahn have shown that Li-poor Li_xSn alloys are formed in SnO and other crystalline oxides at intermediate stages of discharge curve, but evidence for Li-rich Li_xSn phases at deep discharge is speculative.[13] In fact, these latter processes appear very complicated, especially in TCO. At the outset, controversy ensued over the nature of Li uptake in TCO, as the authors implied that Li was incorporated in an "ionic state". Moreover the alloying reaction does not account for all of the (reversible) capacity observed in the TCO glass.

Of equal significance is the role the matrix in TCO plays in the stability of the electrode during charge and discharge, which is not well understood. There have been numerous studies on various tin oxide glasses, most having the stoichiometry $Sn_{1.0}B_xP_yO_z$, as opposed to Al-containing TCO ($Sn_{1.0}B_{0.56}P_{0.4}Al_{0.42}O_{3.6}$).[14,15] The composite matrix has

been presumed to be inert to electrochemical reaction, serving only to maintain the small particle size of the electrochemically active elements.[14] We propose, however, that the "inert" components participate to a greater degree; secondly, the oxygen may play an important role in enhancing the cyclability of the electrode, similar to that observed in molybdenum oxides.[16]

Solid-state NMR is becoming more widely used as an effective tool for probing the reactions occurring within a variety of materials. Several groups have investigated electrochemically active systems, to obtain important and otherwise elusive information about the systems of interest (often glassy in nature). The vast majority of these reports have focussed on positive electrode materials, in particular the manganese spinel $LiMn_2O_4$,[17] and layered $LiCoO_2$.[18] The common denominator among these studies is the paramagnetic nature of the transition metal cation. To date there have been minimal NMR data published on negative electrode materials, especially those that presumably uptake Li *via* an alloying process.[9,19] In contrast to Li intercalation in positive electrode hosts, it is presumed that Li uptake by the electrochemically active metal centres should result in the reduction of those metal centres to an oxidation state of zero, with deep reduction giving rise to clustering of lithium with the active metal centers, and the formation of a particle with metallic properties. The solid-state NMR signal of lithium in such an environment would be dominated by a Knight shift, such as that observed in bulk metals. The Knight shift arises due to the coupling of the magnetic moments of the unpaired conduction electrons at the Fermi level with the nuclear moment.[20] It is dependent on the density of states at the Fermi level.

Here, we provide a detailed analysis of the electrochemical behaviour of SnO and two tin composite oxides, in combination with a complete solid-state NMR study of the cations in these systems. This project was undertaken with the intent of examining whether lithium–tin alloy phases are formed during the reduction of tin containing anodes. We utilized Li solid state NMR anticipating the presence of a Li Knight shift, which would increase in magnitude the further reduced the alloy became (*i.e.* the higher the lithium content the greater the Knight shift). The natural abundance (93%) and high magnetogyric ratio and Larmor frequency of ^{7}Li make it simple to acquire excellent spectra in relatively short periods of time. Unfortunately the quadrupole moment of ^{7}Li is 50 times higher than that of ^{6}Li, resulting in greater quadrupolar broadening, and hence poorer resolution. The low natural abundance of ^{6}Li, however, necessitates the use of enriched materials in the battery. We have investigated the behaviour of lithium within the SnO as well as two tin composite oxides: $Sn_{1.0}B_{0.56}P_{0.4}Al_{0.42}O_{3.6}$ (TCO) and $Sn_{1.5}B_{0.56}P_{0.4}Al_{0.42}O_{4.2}$ (Sn-rich TCO), after electrochemical lithium insertion. As well, by probing the spectator ions in the glass, Al, P, and B, we have been able to shed light on their role in the electrochemical processes.

Experimental

TCO glasses were prepared by grinding stoichiometric amounts of SnO, $Sn_2P_2O_7$, Al_2O_3, and B_2O_3 (Aldrich) and pressing pellets of the mixture into discs. These were arc-melted in an argon atmosphere to produce a completely clear, yellow glass, and subsequently ground and passed through a 625 mesh to yield the active material. Electrochemical studies were performed using a MacPile multichannel galvanostat/potentiostat. The Swagelock™-style cells were assembled in an argon atmosphere, using Li metal, (or 95% ^{6}Li enriched metal) as the counter electrode. Electrodes were cast from a slurry of 80% active material, 5% PVDF binder, and 15% carbon by mass mixed in cyclopentanone. For galvanostatic studies, current-pulse relaxation experiments were performed using a pulse corresponding to insertion of 0.25Li, and allowing the system to achieve equilibrium (defined as a voltage change of less than 4 mV h^{-1}) between steps in the voltage window 0.005–1.5 V.

For preparation of the materials for NMR measurements, Li insertion was performed under potentiodynamic conditions at a discharge rate of 50 mV h^{-1}, on electrodes that typically contained about 5 mg of active material. To ensure equilibration of the samples, the electrodes were held at the desired cutoff voltage for 48 hours before being dried and transferred to NMR rotors in the argon glove box. The rotors were sealed with Kel-F caps that were proven to be airtight by tests with known air-sensitive materials. Solid-state NMR was performed on a Bruker AMX-500 narrow bore magnet, using the resonant frequencies, and reference compounds for the nuclei of interest as follows: ^{6}Li: 73.6 MHz; ^{7}Li: 194.3 MHz ($LiNO_3$ at 0.0 ppm); ^{31}P: 202.4 MHz ($NH_4H_2PO_4$ (ammonium dihydrogen phosphate) at +0.81 ppm from H_3PO_4(aq)); ^{11}B: 160.4 MHz ($NaBH_4$ at 0.0 ppm); ^{27}Al: 130.3 MHz ($Al(NO_3)_3$ at 0.0 ppm) and ^{119}Sn: 186 MHz ($Sn(C_4H_9)_4$ at –6.4 ppm). In all cases, a single pulse-acquire sequence was used. Pulse lengths were typically 2 μs, corresponding to a 30–45° pulse. Delay times of 200 ms were sufficient for the quadrupolar nuclei (^{27}Al and ^{11}B), while 10 s was required for ^{31}P and ^{119}Sn. ^{6,7}Lithium spectra were acquired with delays of 1 s. All spectra were acquired under magic angle spinning (MAS) conditions, using spinning speeds of 5–7.5 kHz. For the boron spectra, background subtraction was carried out to remove the borosilicate glass signal arising from the variable temperature dewar in the MAS probe.

Results

Electrochemical studies

Fig. 1 shows the electrochemical curves for SnO, TCO and Sn-rich TCO on the first cycle, as well as the corresponding cyclic voltammograms (CV). The sharpness of the features in the potentiostatic curve of SnO, as compared to the glassy TCO, is expected for a crystalline *versus* amorphous material. This difference, while implicit in the nature of the materials, illustrates a fundamental cause for the enhanced performance of the TCO glass. Peaks in the potentiostatic curve correspond to specific lithium potential sites within the electrode: following the initial cycle, including the irreversible formation of the lithium oxide matrix, the TCO glass exhibits only a single, broad insertion site, while SnO shows many features. Marked on the cycling curves are the positions at which samples were collected and analyzed using solid-state NMR.

The lithium uptake of SnO, 5.9Li, is close to the theoretical capacity of 6.4Li with a reversible capacity of 3.5Li on the first cycle. TCO achieves an initial lithium uptake of 8.0Li, with a reversible capacity of 4.9 Li/Sn, while Sn-rich TCO reaches an initial lithium uptake of 10.7Li, with a reversible capacity of 6 Li per mole of glass or 4 Li per Sn atom. Comparing these values on first discharge the gravimetric capacities of the three materials are very similar, reaching 1100, 1100, and 1050 mA h g^{-1} respectively.

The CVs for each of the electrochemical curves illustrate the different types of sites being accessed in the crystalline SnO as opposed to the glass TCO materials. The CV for SnO is characterized by two well defined peaks on discharge, at 0.8 V and 0.3 V. There are also several secondary processes at 0.65, 0.45 and 0.2 V on the cathodic sweep. On the anodic sweep, the processes are still well defined, now occurring at 0.45 and 0.65 V, with some smaller features evident between 0.6 and 0.8 V. This contrasts with our observations on the glassy materials. In the latter CVs the processes are much broader and smoother; on discharge peaks are observed at 1.3 V and 0.2 V, with a small feature evident around 0.5 V. On charge a broad

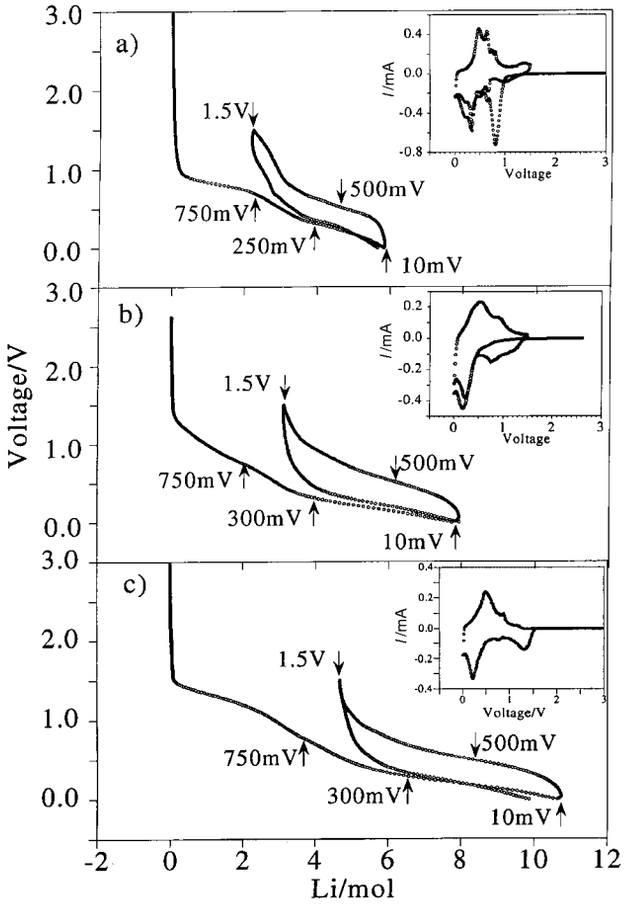

Fig. 1 First discharge/charge/discharge cycle for a) SnO, b) TCO, and c) Sn-rich TCO collected under potentiostatic conditions at 50 mV h^{-1}. Inset: cyclic voltammograms for each electrochemical curve.

feature at 0.5 V along with a smaller feature at 0.85 V is observed. Sn-rich TCO shows somewhat sharper features than TCO itself, due to the enhanced Sn concentration in the former glass. This result shows that the sharpness of the CV features is the result of overall tin concentration, as well as the previously noted differences in crystallinity. The Sn-rich TCO material contains a 50% higher molar concentration of Sn atoms, which are therefore closer to one another than in TCO itself on a statistical basis.

Studies of electrochemically active nuclei—tin and lithium

The ^{119}Sn NMR data for SnO, SnO_2, and TCO are shown in Fig. 2. These spectra were collected at a spinning rate of 8.5 kHz. The spectra of the crystalline tin oxides comprise 1024 scans in each case, whereas the spectrum of the tin composite oxide glass comprises 40 k of scans. Nevertheless, the signal to noise ratio is much worse for the latter spectrum. This is attributed to the very large chemical shift dispersion observed in the TCO spectrum (+100 to –1000 ppm), which arises from the large number of variable tin environments in the glass. Given the internuclear Sn–Sn distance in the glass of approximately 4 Å, the homonuclear dipolar coupling is very weak, and is effectively removed by spinning. The broad Gaussian lineshape in TCO is indicative of the heterogeneity of the Sn environments and spans the regions characteristic of both Sn^{2+} and Sn^{4+}. This suggests that the glass may contain a significant fraction of Sn^{4+}, rather than uniquely Sn^{2+} as previously reported. Auger-XPS data that we have obtained for TCO corroborate this finding. Nevertheless, the discharge capacity of TCO on the first cycle, of 1100 mA h g^{-1}, agrees precisely with that reported by the group from Fuji.

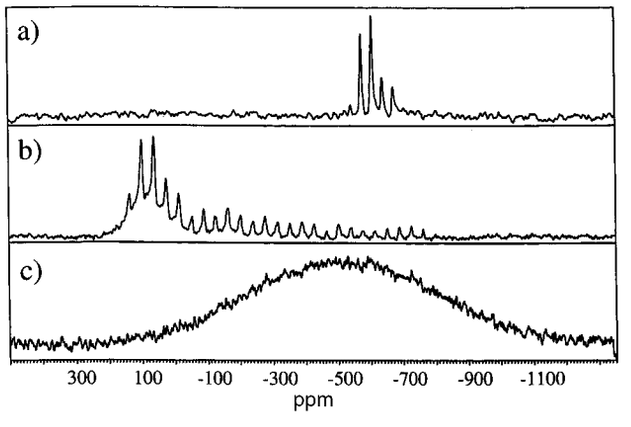

Fig. 2 ^{119}Sn NMR spectra for a) SnO_2, b) SnO and c) TCO.

As well as the possible variation in oxidation state, the coordination environment of tin in TCO glass is also uncertain. The structural implication of a glass is that the coordination environment of the Sn^{2+} is also undetermined, and may range from octahedral through 5 coordinate, and tetrahedral symmetry. In the rutile structure of SnO_2, Sn exists in a distorted octahedral environment, with almost no anisotropy, as reflected in the narrow chemical shift range, −500 to −700 ppm. SnO has a broader chemical shift range, 200 to −800 ppm, and an axially symmetric chemical shielding anisotropy. This is in agreement with the PbO structure type, of which SnO is a member. Somewhat surprisingly, the chemical shift range of TCO is even broader than that of SnO, suggesting that at least some of the tin in TCO exists in environments that differ from that of the parent crystalline oxides. In a study of dioxostannolanes, the chemical shift range of the compounds investigated included chemical shielding anisotropies (CSA) as large as 919 ppm. This example is cited as evidence that large CSA's are found for Sn^{4+} compounds.[21] Unfortunately the structure of the glass is not well enough understood for the authors to comment further on this point. The most significant finding from this brief ^{119}Sn NMR study was that the TCO glass could not be effectively studied by NMR following electrochemical measurements, since the signal to noise ratio of the spectrum, even for a 100 mg sample, was too poor to be useful.

Examination of the materials using ^{6,7}Li solid-state NMR permits a direct probe of the environments that lithium adopts on insertion in the electrode. The results of our ^{6}Li investigation for SnO and TCO during the first electrochemical cycle are shown in Fig. 3. The consistent presence of a narrow peak at ~0 ppm is due to electrolyte, or the surface–electrolyte interface (SEI), and serves as an internal reference in our analysis, although it is not included in our calculations of relative intensities. The deconvolutions of the ^{6}Li MAS NMR lineshapes are summarized in Table 1. On initial discharge to 750 mV (Fig. 3a,e), both the SnO and the TCO show a single narrow signal, shifted to positive frequency with respect to the electrolyte. In SnO (Fig. 3e), this lineshape represents a single contribution at 3.9 ppm with a linewidth of 0.15 kHz. In the case of TCO (Fig. 3a), an effective deconvolution requires two contributions; one at 1.0 ppm with a linewidth of 0.125 kHz, and a second at 2.3 ppm with a linewidth of 0.24 kHz. The first peak observed on discharge corresponds to the formation of the lithium oxide matrix. The shift of 3.9 ppm is close to our experimental value for Li_2O itself (3 ppm). The two peaks in the spectrum of TCO are a reflection of the cation sites in the matrix which presumably arise as a result of the additional elements in the glassy matrix; the first corresponds to Li interacting directly with oxygen while the second corresponds to Li interactions with other glass components. Upon further discharge of SnO to 250 mV (Fig. 3f), the spectrum now includes a broad peak centered at 9.7 ppm in addition to the

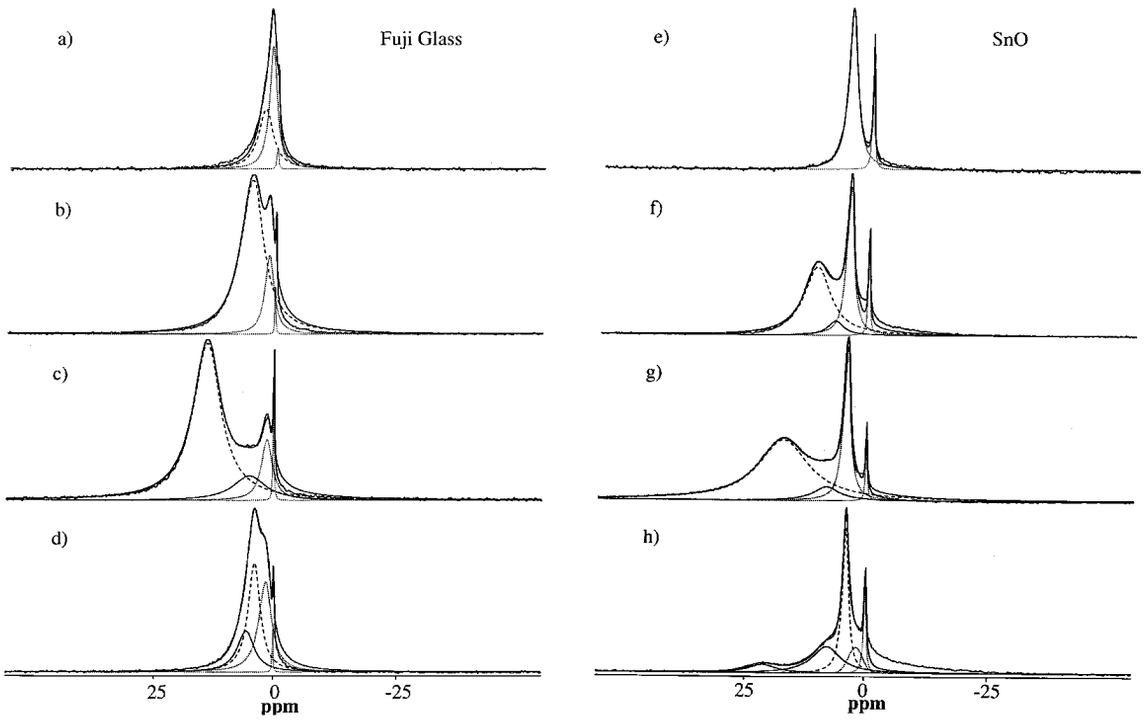

Fig. 3 ^{6}Li spectra for TCO (a–d) and SnO (e–h) and at various levels of discharge: a,e) 750 mV; b,f) 300 mV; c,g) 10 mV on discharge; and d,h) 500 mV on charge.

sites present earlier in the discharge. The TCO electrode discharged to 300 mV (Fig. 3b) also includes a new broad feature, although its shift is only 4.5 ppm. At full discharge (Fig. 3c,g), these new broad features continue to move to higher frequency; in SnO to 15.5 ppm with a linewidth of 0.83 kHz, and in TCO to 12.6 ppm with a linewidth of 0.46 kHz. These lines represent 68% and 75% of the total non-electrolyte Li intensity, respectively. These additional signals are attributed to interaction of Li with predominantly Sn centres (*vide infra*), a contribution that grows in relative intensity as well as increasing in chemical shift as the cell reaches deepest discharge (maximum lithium concentration). Upon charge to 500 mV, the SnO and TCO respond quite differently. In the case of SnO (Fig. 3h), the dominant peak becomes the original 3.7 ppm peak, which represents 40% of the overall intensity. As well, resonances at 7.1 ppm (33%) and 18.9 ppm (11%) account for a portion of the spectral intensity. While the latter still represents a small fraction of the total content, it is significant that this peak does not move from its high frequency position on charge. In the case of TCO, however, following the removal of 1/3 of the Li (500 mV on charge), the peaks shift to lower frequency, *i.e.* toward their original positions during the initial discharge (Fig. 3d). The most intense peak occurs at 3.7 ppm (41%), while the highest frequency peak is only 1.4 ppm higher, at 5.1 ppm (22%). Therefore, it appears that the Li–Sn contact established at deepest discharge is more reversible in the case of the TCO glass than for SnO. The contrasting behaviour between the two oxides is indicative of the relative ionicity of the interactions between lithium and tin in the materials.

None of the chemical shift values observed in the electrode materials correspond to significant Knight shifts, as expected if the lithium is undergoing a true alloying process to form LiSn phases. The maximum shift observed for any of the electrodes on the first cycle was $\sim$15 ppm; far less than the 114 ppm shift observed for a bulk $Li_{22}Sn_5$ alloy.[9,19] Fig. 4 shows ^{7}Li spectra for SnO, TCO and Sn-rich TCO at full discharge following 5 cycles, 10 cycles and 10 cycles, respectively. It was surmised

Table 1 Deconvolutions of ^{6}Li spectra including peak positions, linewidths, and relative intensities excluding the electrolyte contribution

TCO				SnO			
Electrode	Shift/ppm	Width/Hz	Intensity (%)	Electrode	Shift/ppm	Width/Hz	Intensity (%)
750 mV	0.0	19		750 mV	0.0	30	
	1.0	125	52		3.9	150	100
	2.3	240	48				
300 mV				250 mV	0.1	26	
	0.1	11			3.7	117	34
	1.2	147	17		6.2	257	7
	4.5	377	83		9.7	434	59
10 mV	0.1	16		10 mV	0.0	26	
	1.3	180	11		3.8	113	24
	4.6	541	14		7.5	426	8
	12.6	459	75		15.5	832	68
500 mV charge	0.1	13		500 mV charge	0.0	39	
	1.6	210	37		1.7	228	16
	3.7	197	41		3.7	101	40
	5.1	278	22		7.1	460	33
					18.9	468	11

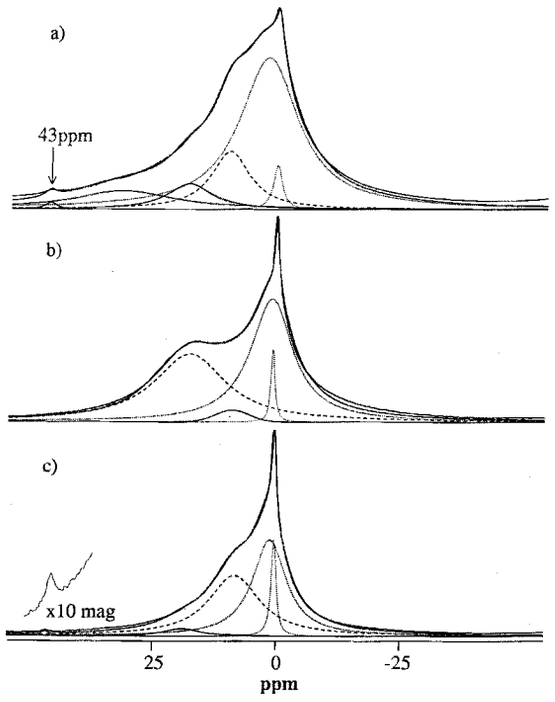

Fig. 4 ^{7}Li spectra for cycled samples at 10 mV on discharge for a) SnO following 5 cycles, b) TCO following 10 cycles and c) Sn-rich TCO following 10 cycles.

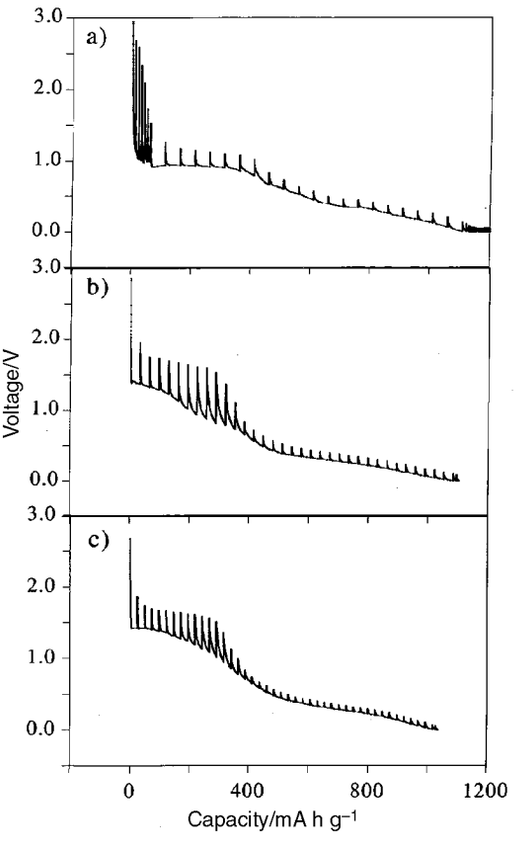

Fig. 5 Galvanostatic intermittent titration curves for a) SnO, b) TCO, and c) Sn-rich TCO.

that the alloy phases, while not formed on the initial discharge, might develop upon repetitive cycling of the electrodes. Significant differences are evident in these spectra. First and foremost, the TCO glass spectrum remains almost unchanged after 10 cycles. The spectrum is readily deconvoluted into 4 contributions, with the highest shift to 16 ppm. This shift to higher frequency may correspond to an increasing Li–Sn contact, but it is a modest change from the shift of 12.6 ppm observed in the ^{6}Li spectrum on initial discharge. Contrasting results are seen in the case of SnO. While the shift never reaches a value of greater than 100 ppm, as expected for the most lithium rich alloy, the deconvolution of this spectrum reveals a complicated set with peaks ranging from 8 to 43 ppm. The spectrum of Sn-rich TCO following 10 cycles is an intermediate case, in which a small peak at 43 ppm is discernable, but is much weaker than the corresponding peak observed in SnO following only 5 cycles.

Electrochemical probe of kinetic response

The kinetic responses of the electrode materials were examined using a Galvanostatic Intermittent Titration Technique (GITT). During such an experiment, current pulses are applied to the system. These are separated by a relaxation period, during which the cell is put in open circuit to allow equilibrium to be established. The pulse time has been chosen to allow 0.25Li to react with the active material and the open-circuit voltage (OCV) is monitored until the potential varies by less than 4 mV h^{-1}. At this point the system is close to equilibrium and the next titration step is initiated. During the pulse the potential of the system departs from the equilibrium potential, owing to structural and/or kinetic hysteresis. During the open-circuit step the potential relaxes towards equilibrium. As a consequence, the larger the potential variance from the equilibrium OCV, the further the system is perturbed from equilibrium during the pulse, demonstrating that the kinetics are slower under these conditions.

The results of the GITT experiments for each material are shown in Fig. 5. The curves in all cases show two distinct regions, characterized by the amplitude of the potential variation during the relaxation period. The region from 0 to approximately 400 mA h g^{-1} shows the slowest kinetic response. This process ends at the completion of Li_2O matrix formation which is correlated with the insertion of the first 2 lithiums into SnO, or the first ~3 Li into TCO and Sn-rich TCO. The second process continues to the end of discharge. The latter process is facile, as indicated by the small amplitude of the potential variation observed here for all three materials.

The differences between the TCO glasses and SnO itself are most significant during the early stages of discharge. In the TCO materials, this portion of the GITT curve is characterized by a large potential variation during OCV corresponding to long relaxation periods. This is indicative of a kinetically inhibited electrochemical process; one which is far from equilibrium. In the tin composite oxide glasses, two general processes are evident, but the first process appears to be separable as two secondary processes, distinguished by a slight change in slope as well as deeper relaxation periods at lithium insertion levels of greater than 1Li. In TCO the first process exhibits potential variations of 0.5 V up to 1Li, and subsequently ~0.9 V up to 2.5Li. In Sn-rich TCO, the first portion of the curve is characterized by potential variations of 0.4 V, which deepen slightly beyond 1Li to ~0.5 V. In SnO, the GITT curve is flat during the first process and the amplitude of the potential variance is typically 0.3 V. From these results we observe that the rearrangement of the glass, concurrent with the reduction of $Sn^{2+/4+}$ to Sn^{0}, is more kinetically inhibited than the reaction of SnO with Li to form Sn metal and Li_2O. There is a change in slope at about 2–3 Li, beyond which the lithium insertion process becomes much easier. This is evident from the more facile kinetic response in this latter portion of the electrochemical process. In this portion of the GITT curves, the three materials respond similarly. In the TCO glasses beyond 3Li, the amplitudes of the potential variations become smaller, reaching an average value of 0.1 V. As the

second process begins in SnO, the potential variations are reduced ($\sim$0.15 V), and are maintained at this value throughout the remainder of the discharge process.

Participation of electrochemically inactive components

An inherent assumption in the discussions of the TCO glass to date has been the inconsequential role of the Al, B, and P ions in the structure. The premise has been that these 'spectator' ions simply prevented aggregation of the Sn atoms following discharge, and other than that were inert. Solid-state NMR permits investigation of the role that the spectator ions play (if any) in the structural rearrangements occurring during the electrochemical reaction with lithium. Fig. 6 shows the ^{27}Al MAS NMR spectra collected for TCO at the same various potentials studied using ^{6,7}Li NMR. It is clear from these data that the Al coordination changes throughout the charge and discharge processes. The pristine glass itself shows two types of Al sites, namely octahedral (centered at 0 ppm) and five-coordinate (centered at 35 ppm). On discharge the changes in the coordination environment at the aluminium centres are evident from the variations of the peak positions. The peaks are never clearly resolved owing to the glassy nature of the active material, but at 750 mV the aluminium coordination environment clearly changes from octahedral towards tetrahedral (resonance at 80 ppm). This trend continues throughout the discharge sweep, and is subsequently reversed on charge. The sharpness of the peak that appears at 0 ppm (500 mV on charge) indicates the creation of some moderately crystalline or well-ordered regions. Further charging to 1.5 V shows that this crystallization is limited, however, and the reappearance of the five-coordinate Al site suggests that the basic glassy framework is regenerated to some extent. Even more important, following 15 cycles of the cell, despite the significant changes that occur in the glass during charge and discharge, the spectrum at the bottom of discharge is remarkably similar to that observed at the end of the first cycle. The local Al–O environment can thus sustain reversible changes, suggesting a high degree of adaptability in the bonding. The ^{27}Al spectrum of pristine Sn-rich TCO shows the same two features as TCO itself, corresponding to octahedral and five-coordinate Al, and upon discharge to 10 mV, again the spectrum is similar to that found for TCO.

Fig. 7 shows the ^{31}P MAS NMR spectra collected for the glass at the same points in the TCO electrochemical cycle as those chosen for ^{27}Al. The pristine glass exhibits a single broad ^{31}P signal, centered at –16 ppm. This shift correlates to signals observed for crystalline aluminium, boron, and tin phosphates.[22] The broadness arises from the amorphous nature of this sample. On discharge to only 750 mV, the ^{31}P spectrum becomes extremely broad, and a peak at 12 ppm is barely observable. The chemical shift value matches that observed for crystalline lithium phosphates.[22] Significant structural changes occur in the glass at this stage. Upon further discharge the 12 ppm peak narrows, hence gaining intensity. During the charge cycle a new resonance appears at –12 ppm. This sharp peak, which increases in intensity upon further charging to 1.5 V, represents the formation of crystalline phosphate regions during the oxidation process. At the bottom of discharge following the 15th cycle of the cell, the ^{31}P spectrum contains only the previously observed peak at +16 ppm, with no evidence of the crystalline component. Both the ^{27}Al and ^{31}P NMR results indicate the formation of some crystalline domains within the electrodes upon charge. This crystallite formation appears to be reversible during the first 15 cycles, but would likely become irreversible upon extended cycling, thus compromising the battery lifetime.

The corresponding ^{11}B MAS NMR spectra of the TCO glass are displayed in Fig. 8. The pristine glass spectrum contains sharp features, including contributions from tetrahedral B sites, as well as trigonally coordinated B. The sharp features from tetrahedral boron disappear upon discharge to 750 mV,

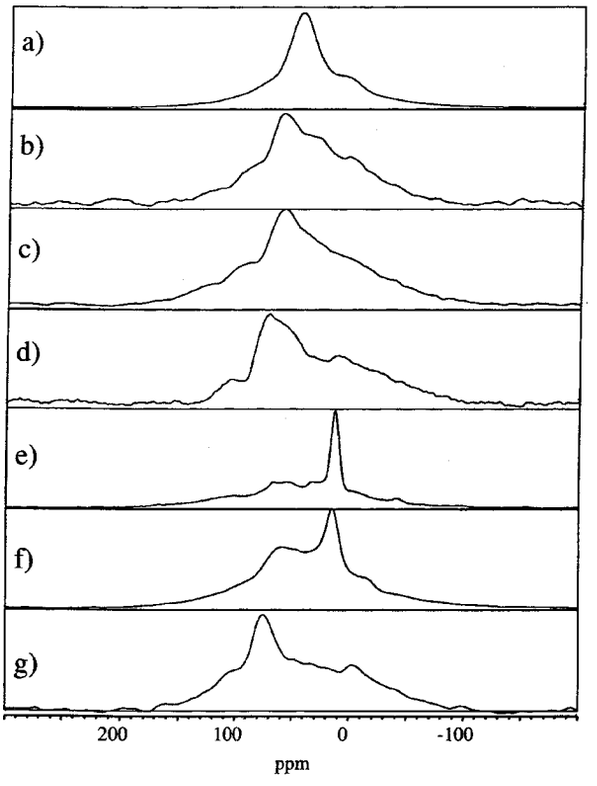

Fig. 6 ^{27}Al spectra for a) pristine TCO and TCO electrodes at b) 750 mV, c) 300 mV, d) 10 mV, on discharge and e) 500 mV, f) 1.5 V on charge, and g) 10 mV following 15th cycle.

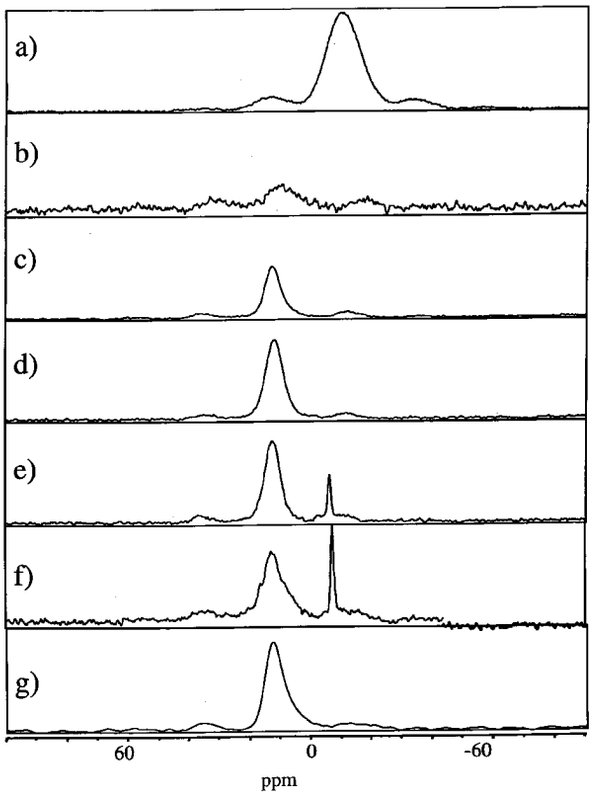

Fig. 7 ^{31}P spectra for a) pristine TCO and TCO electrodes at b) 750 mV, c) 300 mV, d) 10 mV, on discharge and e) 500 mV, f) 1.5 V on charge, and g) 10 mV following 15th cycle.

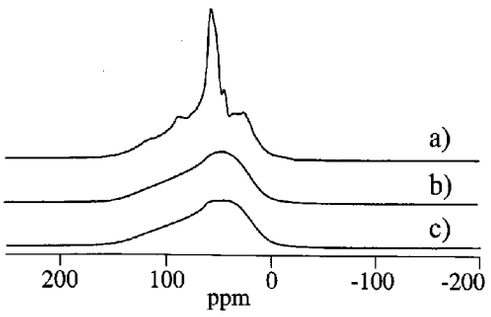

Fig. 8 ^{11}B spectra for a) pristine TCO and TCO electrodes at b) 750 mV, c) 10 mV.

leaving only a broad peak centered at 0 ppm. Characterized by broad featureless lineshapes, the ^{11}B MAS NMR spectra acquired upon further cycling do not change from that observed at 750 mV.

Discussion

The 1997 report of Li insertion into TCO demonstrated that the electrochemical performance of the glass was enhanced compared to that of crystalline SnO,[2] and also suggested that the reaction mechanism was one of insertion as opposed to an alloying process. In view of the extensive studies that have appeared recently suggesting that the fundamental process in tin oxides must involve the reaction of lithium with tin centres to a maximum stoichiometry of $Li_{22}Sn_5$, it is evident that the mechanism of reaction is at issue. It is also unclear precisely what allows TCO glass to exhibit such improved electrochemical response compared to SnO. Our studies presented here shed light on the mechanisms at work in these very different materials. The unique insights gained include an understanding of the interplay between the lithium and tin centers; the role of thermodynamics in this process; and evidence for the participation of framework cations in the reversible reactions within the electrode.

Absence of Knight shifts—implications for particle size and surface energy

Although no direct calculation of particle size is possible from lithium NMR, the data support our contention that the size of the active centres within these materials is limited as we will discuss below. Two general observations from the $^{6,7}Li$ NMR data are significant. First, the absence of a Knight shift is notable, as it indicates that lithium is not present in a metallic environment, such as an alloy. We and others have documented the shift of $Li_{22}Sn_5$ to be on the order of 100 ppm.[9,19] If the formation of bulk lithium–tin alloy particles occurs on deep discharge, this would be clearly visible in this region of the $^{6,7}Li$ NMR spectra. Also crucial is the study of the cycling behaviour of these electrodes, where the differences in the number and positions of discernable contributions to the Li NMR spectra demonstrate the reasons for the enhanced cyclability of the glass.

The majority of previous work in the area of Knight shift phenomena has focused on bulk metals, alloys or intermetallics, where the smallest particle sizes encountered were in the formation of micron-sized lithium metal particles within a LiF crystal;[23] there is also a set of unpublished data on alkali clusters.[24] In the materials studied here, the particles formed on discharge to 10 mV (2Li) are only about 30 Å for TCO, and 175 Å for SnO, based on X-ray linewidth broadening.[25] The question arises whether the Knight shift mechanism is inhibited in particles of such small size. In the case of particles formed *in situ* within an oxide framework, there are two interdependent reasons for the observed shifts. First, if the surface/volume ratio of the particles is sufficiently large (*i.e.*, the particles are very small) the proximity of electronegative oxygen in the matrix and large fraction of M–O bonds on the surface of the particle will reduce the electron density, leaving the lithium more electron-poor than it would be in an alloy particle embedded in a metal matrix. Second, the size of the Li–Sn nanophase may be small enough to prevent the free motion of conduction electrons that would be possible in a bulk metal, hence eliminating the possibility of a true Knight shift. Inevitably these two factors are equally significant.

Initially, we observe the formation of a lithium oxide matrix in both materials. The ^{6}Li NMR spectrum of TCO at 750 mV is deconvoluted into 2 overlapping contributions. This arises from the various types of Li–O–X interactions possible in TCO glasses, as opposed to the unique Li–O–Sn interaction present in SnO. Further discharge to an intermediate level of reduction reveals the presence of a Li–Sn interaction. This resonance is shifted to higher frequency as the lithium concentration increases. The oxide-rich matrix affects the Li–Sn interaction, as the presence of extensive M–O bonding at the particle surface would polarize electron density away from Li. Besides mediating the character of the Li–Sn interaction, the matrix also limits the aggregation of Sn particles and provides a reservoir of accessible lithium. At the point of deepest discharge the Li–Sn interaction dominates the spectra in both cases and results in a shift to even higher frequency, with the SnO phase showing a higher shift than that of TCO. We suggest that this interaction represents a lithium–tin 'nanophase' with proximal oxide, in which the particle size is small enough to prohibit the free motion of conduction electrons. We conclude that the observed resonances are not true Knight shifts, but rather chemical shifts, the magnitudes of which are affected by the particle size. The issue of particle size is a difficult one, as we have no direct method of measuring the size of the domains. Since the observed shifts for Li–Sn in SnO exceed those of TCO at deepest discharge, it is likely that the nanophases formed in the SnO electrodes are somewhat larger than those created in TCO. We believe that the ability to maintain small Li–Sn domains is a key feature in the cyclability of the TCO material.

Upon charging the cells to 500 mV the differences in the ^{6}Li NMR spectra give vital clues as to the origin of the enhanced cyclability of TCO. The immediate shift of the TCO peaks to low frequency after even a partial charge is indicative of the dissolution of the Li–Sn interaction, whereas the persistence of peaks at higher chemical shift in SnO demonstrates that these interactions are maintained to a greater extent. This suggests that in TCO, there is intimate contact between the oxide matrix and the Li–Sn nanophases, which is only possible if the particles are in the cluster-size regime. These results also suggest that it is the ability of the TCO framework to readily undergo structural rearrangement that allows it to cycle more reversibly than SnO.

The structural adaptability proposed here is congruent with the observed ^{7}Li NMR behaviour on cycling, in which more substantial Li–Sn contacts at 43 ppm were observed in the SnO electrode after extended cycling. The latter is an important signature, as a similar peak was observed in a bulk synthetic $LiSn/Li_{2.3}Sn$ alloy mixture prepared at high temperature. This indicates that the formation of Li–Sn domains is favoured in SnO, and may therefore lead to detrimental effects upon cycling. As well, the serendipitous aging of several SnO and SnO_2 electrodes also resulted in the appearance of this signature peak. The fact that it is not observed in the TCO spectra, even following 10 cycles of the cell, is further evidence that the Li–Sn domains are limited in size in TCO, whereas these domains are able to grow in SnO. This size-limiting mechanism appears to be the key to improved electrochemical properties.

Thermodynamic arguments predict that in bulk phases the

reaction between lithium metal and tin oxide should result in the formation of lithium oxide and tin metal. Based on the Gibbs free energy of this reaction, it should be spontaneous in the forward direction, and hence irreversible unless equivalent energy is imparted to the system to drive the reaction in the reverse. This is indeed the case for bulk materials. We propose that the reactions occurring within the TCO glass are taking place in a size-limiting regime. Hence, the thermodynamics are strongly affected by the high surface energy of the particles, namely by the surface reactions that occur spontaneously between lithium, tin and oxygen. The reaction between lithium and tin, which is stoichiometrically controlled from a macroscopic perspective with a maximum lithium content corresponding to the most lithium-rich Li–Sn line phase, is also much more complex on a microscopic level. The model we propose is that the tin clusters formed on reduction of the cell are in close proximity with both lithium and oxygen as a result of these particles having a very high surface area : volume ratio. As the concentration of lithium in the electrode increases, the lithium–tin interaction will necessarily increase, but this makes no requirement for the interaction to be that of a true lithium–tin compound phase. In fact, the kinetics of the system inevitably limit the formation of microcrystalline phases at ambient temperature, even in tin oxide itself. As well, the surface energy of these particles allows the "back-reaction" of lithium with oxygen to be reversible at a lower potential than predicted from simple considerations that exclude surface energy contributions. Our EXAFS studies of these systems have also shown proof of this.[19] The proximity and availability of oxygen in the host matrix is surmised to enhance the reversibility and cyclability of the cell. Availability of matrix bound oxygen will be determined by the surface energy of the electrochemically active particles, hence the smaller the aggregates, the more reactive they will be.

Role of spectator ions

Evidence for the role of the components of the oxide matrix in these materials is provided by the solid-state NMR studies performed on the 'spectator ions'. Our results from ^{31}P and ^{11}B NMR strongly suggest that lithium inserts not only into Sn–O–Sn bonds, but also into Sn–O–X bonds, and X–O–X bonds, where X is Al, B, or P in the composite glasses. The ^{31}P NMR spectrum, which displays a well-resolved peak for the pristine glass, is transformed into a very broad signal at 750 mV (equivalent to insertion of 2 Li), indicative of dramatic structural changes in the phosphate environments. If, on discharge, signal intensity at the original position had been maintained along with the appearance of a peak at +12 ppm (Li_3PO_4), this would have been evidence for preferential reaction of lithium with the Sn–O–P bonds in the glass which leaves the X–O–P bonds intact. The results, however, indicate that even partial lithium insertion causes an all-encompassing rearrangement of the glass. Our interpretation is corroborated by the changes in the ^{11}B spectra. In the pristine glass there are two distinct boron environments, whereas in the 750 mV electrode material the tetrahedral site has been removed, leaving only a broad, featureless lineshape, corresponding to trigonally coordinated boron. Again, the NMR spectra reveal the drastic structural rearrangements that occur in the glass during the insertion of the first 2–3 moles of Li. We note that other recent IR studies of Li insertion into SnO–P_2O_5–B_2O_3 glasses have provided a similar conclusion.[15]

Our interpretations are strongly supported by the GITT measurements; particularly in the first portion of the GITT curve for each material. A single process occurs in the case of SnO, however the TCO curves can be considered to undergo two distinct processes during the insertion of the first 2–3 equivalents of Li. To explain this observation we can consider the types of bonds that are broken and reformed in each case. For SnO, Li can only insert into the Sn–O–Sn bond, whereas the TCO network comprises both Sn–O–X as well as X–O–X interactions, where X = Al, B or P. It is questionable as to whether the lithium should be expected to insert into an X–O type bond, but both our GITT data and several of the NMR spectra of the 'spectator ions' point to this conclusion. The GITT results for TCO indicate that the insertion process up to the first 2–3 Li is much more kinetically inhibited than the equivalent process in SnO. If the lithium were selectively inserted into Sn–O bonds in both cases, the kinetics of the reactions would be expected to be equivalent. On this basis, it seems likely that the lithium is not selective, but reacts as well with the other bonds present. The fact that these oxides themselves are electrochemically inert suggests that the reason for the slow kinetics is the initial step as the glass is rearranged.

The ^{27}Al NMR results similarly demonstrate the flexibility of the oxide framework. Changes in the coordination environment from predominantly five-coordinate in the pristine glass, toward tetrahedral upon discharge, and then back toward octahedral upon charge are clearly evident. The adaptability of the multi-component framework may allow for the facile movement of oxygen within the structure, and thus expedite the reaction of the lithium with tin in the TCO glass and accommodate the reversibility of this process.

Acknowledgements

Funding was provided by NSERC in the form of research, equipment and collaborative grants (LFN, WPP) and a postgraduate scholarship (GRG). The authors also thank Jim Garrett (Brockhouse Institute for Materials Research, McMaster University) for his help in preparing the TCO glasses.

References

1 Y. Idota, Fuji Photo Film, *Eur. Pat.* 651, 450A1, 1995; *Can. Pat.* 2 113 053, 1995; Y. Idota, *US Pat.*, 5 478 671, 1995.
2 Y. Idota, T. Kubota, A. Matsufuji, Y. Maekawa and T. Miyasaka, *Science*, 1997, **276**, 1395.
3 J. Yang, M. Wachtler, M. Winter and J. O. Besenhard, *Electrochem. Solid State Lett.*, 1999, **2**, 161; J. Yang, M. Winter and J. O. Besenhard, *Solid State Ionics*, 1996, **90**, 281; J. O. Besenhard, M. Hess and P. Komenda, *Solid State Ionics*, 1990, **40–41**, 525.
4 O. Mao, R. L. Turner, I. A. Courtney, B. D. Fredericksen, M. I. Buchett, L. J. Krause and J. R. Dahn, *Electrochem. Solid State Lett.*, 1999, **2**, 3; O. Mao and J. R. Dahn, *J. Electrochem. Soc.*, 1999, **146**, 423 and references therein.
5 K. D. Kepler, J. T. Vaughey and M. M. Thackeray, *Electrochem. Solid State Lett.*, 1999, **2**, 7.
6 I. A. Courtney and J. R. Dahn, *J. Electrochem. Soc.*, 1997, **144**, 2045; I. A. Courtney, W. R. McKinnon and J. R. Dahn, *J. Electrochem. Soc.*, 1999, **146**, 59.
7 W. Liu, X. Huang, Z. Wang, H. Li and L. Chen, *J. Electrochem. Soc.*, 1998, **145**, 59.
8 T. Brousse, R. Retoux, U. Herterich and D. M. Schleich, *J. Electrochem. Soc.*, 1998, **145**, 1; T. Brousse, S. M. Lee, L. Pasquereau, D. Defives and D. M. Schleich, *Solid State Ionics*, 1998, **113–115**, 51.
9 Y. Wang, J. Sakamoto, C. K. Huang, S. Surampudi and S. G. Greenbaum, *Solid State Ionics*, 1998, **110**, 167.
10 W. G. Moffat, *The Handbook of Binary Phase Diagrams*, Schenectady, NY, 1990; D. A. Hansen and L. J. Chang, *Acta Crystallogr., Sect. B: Struct. Crystallogr. Cryst. Chem.*, 1978, **25**, 2392; U. Frank and W. Muller, *Z. Naturforsch., Teil B*, 1975, **30**, 316 and references therein.
11 J. Wang, I. D. Raistrick and R. A. Huggins, *J. Electrochem. Soc.*, 1986, **133**, 457; B. A. Boukamp, G. C. Lesh and R. A. Huggins, *J. Electrochem. Soc.*, 1981, **128**, 725.
12 T. Landolt-Bornstein, in *Structural Data of Elements and Intermetallic Phases*, vol. 6, Springer, Berlin, 1971.
13 J. R. Dahn, I. A. Courtney and O. Mao, *Solid State Ionics*, 1998, **111**, 289; I. A. Courtney, J. S. Tse, O. Mao, J. Hafner and J. R. Dahn, *Phys. Rev. B*, 1998, **58**, 1583.

14 I. A. Courtney and J. R. Dahn, *J. Electrochem. Soc.*, 1997, **144**, 2943.
15 S. Machill, T. Shodai, Y. Sakurai and J. Yamaki, *J. Solid State Electrochem.*, 1999, **3**, 97; S. Machill, T. Shodai, Y. Sakurai and J. Yamaki, *J. Power Sources*, 1998, **73**, 216.
16 F. Leroux, G. R. Goward, W. P. Power and L. F. Nazar, *Electrochem. Solid State Lett.*, 1998, **1**, 255; F. Leroux, G. R. Goward, L. F. Nazar and G. Ouvrard, *J. Phys. Chem.*, submitted.
17 Y. J. Lee, F. Wang and C. P. Grey, *J. Am. Chem. Soc.*, 1998, **120**, 12601.
18 M. Carewska, S. Scaccia, F. Croce, S. Arumugam, Y. Wang and S. Greenbaum, *Solid State Ionics*, 1997, **93**, 227; C. Marichal, J. Hirschinger, P. Granger, M. Ménétrier, A. Rougier and C. Delmas, *Inorg. Chem.*, 1994, **34**, 1773.
19 G. R. Goward, W. P. Power, F. Leroux, G. Ouvrard, W. Dmowski, T. Egami and L. F. Nazar, *Electrochem. Solid State Lett.*, 1999, **2**, 367.
20 C. P. Slichter, *Principles of Magnetic Resonance*, Springer Verlag, Berlin, 1978.
21 T. B. Gindley, R. E. Wasylishen, R. Thangarasa, W. P. Power and R. D. Curtis, *Can. J. Chem.*, 1992, **70**, 205.
22 T. M. Duncan, *A Compilation of Chemical Shifts of Anisotropics*, AT&T Bell Labs, Madison, Wisconsin, 1990.
23 G. C. Carter, L. H. Bennett and D. J. Kahan, *Metallic Shifts in NMR; Progress in Materials Science*, vol. 20, Pergamon Press, Oxford, 1977.
24 J. M. Snowel, PhD Dissertation, Yale University, 1993.
25 G. R. Goward, PhD Dissertation, University of Waterloo, 1999; G. R. Goward, W. Dmowski, T. Egami and L. F. Nazar, unpublished results based on X-ray scattering experiments at the NSLS, Brookhaven.